Ejected electron spectrum of He below the $N=2$ threshold

B. A. deHarak, J. G. Childers,* and N. L. S. Martin
Department of Physics and Astronomy, University of Kentucky, Lexington, Kentucky 40506-0055, USA
(Received 21 June 2006; published 29 September 2006)

Electron-impact ejected electron spectra of He below the He^+ $N=2$ threshold have been measured for all combinations of incident energies 550, 150, and 75 eV and ejected electron directions 60°, 90°, and 120° with respect to the incident electron beam direction. Autoionizing levels from the four main series $^1S^e_0$, $^3P^o_1$, $^1D^e_2$, and $^1P^o_1$, are observed up to $n=7$, and resolved up to $n=5$. In addition several weak members of other series are observed. The positions, and in some cases the widths, are tabulated for 30 levels, and these are compared with theoretical and other experimental values.

DOI: 10.1103/PhysRevA.74.032714 PACS number(s): 34.80.Dp

I. INTRODUCTION

The spectrum of helium from an excitation energy of 57 eV to the He^+ $N=2$ threshold at 65.4 eV contains many Rydberg series of autoionizing levels embedded in the He^+ $1sE\ell$ continuum. Only the five lowest levels $2s^2\,^1S_0$, $2s2p\,^3P$, $2p^2\,^1D_2$, $2s2p\,^1P_1$, and $2p^2\,^1S_0$ may be described in a single-configuration approximation. For the higher members of these series, and all members of other series, the strong electron-electron correlation effects present in He preclude a single-configuration description and the $(sp,2n\pm)$ scheme (originally called the $(2n\pm)$ scheme [1]) may be used for the optically allowed series while the ${}_N(K,T)^A_n$ classification scheme [2] (also written as ${}_n(K,T)^A_N$ [3–5]) may be used for both optically allowed and optically forbidden series. The quantities K,T correspond to angular and A to radial correlations of the two electrons in a hyperspherical-coordinate description of He. A discussion of these schemes is given in Ref. [5], for example.

Since the *number* of basis states is the same in any classification scheme, it is possible to use the familiar single-configuration basis to predict the number of $(sp,2n\pm)$ or ${}_N(K,T)^A_n$ Rydberg series for a given L,S. Thus, for example, the number of $^1D^e$ series that contain $n=2$ is one, corresponding to the configuration $2p^2$. For $n=3$ there are two series corresponding to the basis configurations $2p3p$, $2s3d$, and for $n\geqslant 4$ there are three series corresponding to a $2pnp$, $2snd$, $2pnf$ basis. (Note that correlation effects do not affect the validity of the LS coupling scheme used, but that at very high n, spin-orbit effects become significant [6].) Figure 1 gives the positions (up to $n=6$ or 7) of all 16 series for $L\leqslant 2$; the $n=2$ positions are experimental [7] and the remainder are calculated values [2].

The most prominent of the dipole-allowed series, $(sp,2n+)$, was first seen in the pioneering synchrotron experiments of Madden and Codling [8]. Since then all three dipole-allowed series have been extensively studied up to high n with high-resolution absorption experiments using synchrotron radiation [9,10], and the $(sp,2n\pm)$ series have also been observed in high-resolution photoelectron experiments [11]. Recently, the $2p^2\,^1D_2$ *quadrupole* level has been observed in a photoelectron experiment via dipole-quadrupole interference effects [12]. Other synchrotron experiments have investigated the effect of applied electric fields on the spectrum of He below the $N=2$ threshold [13,14] and Stark mixing has been used to observe optically forbidden even-parity $^1P^e$ levels in photon-induced fluorescence spectra [15].

The four lowest $n=2$ levels, $2s^2\,^1S_0$, $2s2p\,^3P_1$, $2p^2\,^1D_2$, and $2s2p\,^1P_1$, have been extensively studied in a variety of charged-particle-impact experiments using electron, proton, and ion projectiles. The electron impact experiments fall into three main categories: energy loss [16,17], ejected electron [18,19], and $(e,2e)$ [20–23], where—in addition to the singlet levels—the triplet level may be seen at low incident energy. Energy loss spectra also contain nonautoionizing levels such as $2p^2\,^3P$ [24]. Postcollision interaction (PCI) effects for incident electron energies less than 10 eV above threshold cause line-shape distortion and a shifted resonance energy [25,26]. Such PCI effects can also be very important in ion- [27,28] and proton- [29] impact experiments.

There is less experimental data on the $n>2$ optically forbidden levels. In an ion-atom collision experiment a survey spectrum for Li^++He showed some $n=3$ levels, but the reso-

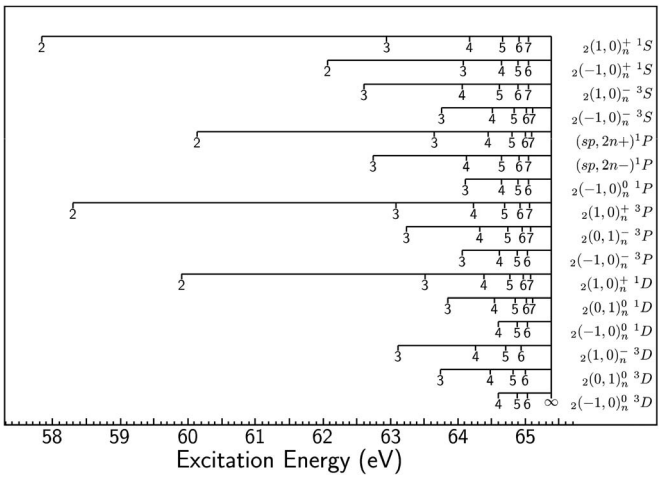

FIG. 1. Level positions above the helium ground state of the 16 He doubly excited series with $L\leqslant 2$ that lie below the $N=2$ threshold.

*Present address: Department of Physics, California State University, Fullerton, CA 92834-6866, USA.

lution was insufficient to resolve them [28]. Levels up to $n=5$ (resolved up to $n=4$) have been identified in an experiment that created autoionizing levels by double electron capture of low-energy He^{2+} ions colliding with Ba atoms [30], and the energies of some levels up to $n=5$ have been extracted from vacuum ultraviolet VUV photoemission studies [31]. Because of the nature of these two experiments there was no line-profile information and the intensity variation with increasing n of well-behaved Rydberg series, associated with charged-particle-impact spectra, was not present. In addition, the data of [30] included PCI effects which precludes the extraction of accurate level energies.

There is one detailed electron-impact study which includes the $n>2$ optically forbidden levels [18]. Levels up to $n=5$ are tabulated, but only levels up to $n=3$ were resolved. Because of the low count rates associated with the small helium cross section, the statistics of these experiments were relatively poor. In the present work, our apparatus incorporates a position-sensitive detector (PSD) which results in an effective count rate more than an order of magnitude higher than those obtained in earlier experiments. Thus the experiments presented in this paper represent an advance over those of Ref. [18] because the improved statistics of our spectra, taken with a PSD, enable weak features, not seen in their work, to be observed, and also enable the resolution of closely spaced features. The good statistics of our data allow us to fit line profiles to obtain accurate profile parameters and enable the accurate manipulation of two spectra taken at different ejected electron directions.

In Sec. II we give details of the experimental method, in Sec. III we present and discuss the experimental results, and Sec. IV contains the summary and conclusions.

II. EXPERIMENTAL METHOD

The present He ejected electron experiments use part of an $(e,2e)$ apparatus which has been described in detail elsewhere [32]. An unmonochromated electron gun intersects a gas beam that effuses through a 1-mm-diameter aperture approximately 2 mm below the interaction region. The ejected electron detector, which uses a hemispherical-sector electrostatic-type analyzer terminated in a position-sensitive detector, is mounted on a turntable. During an experiment energies are scanned repetitively to minimize the effect of any drift in, for example, the electron beam intensity. Each scan took approximately 1 h and consisted of stepping through 1250 points in 7.5 meV increments. Each spectrum presented in this paper took between one and four days to acquire.

The energy resolution of the present He spectra is just under 50 meV, somewhat larger than the 40 meV obtained in heavier targets [32]. We believe that the inferior resolution in helium is due, at least in part, to Doppler broadening. Although the helium beam emerges from a thin tube of length 10 mm and diameter 1 mm, and is therefore fairly well collimated, there is a substantial background He pressure of $\sim 10^{-5}$ Torr. (Experiments are carried out at the maximum possible beam intensity in order to maximize the count rates from small e-He cross sections.) For an electron ejected with energy E_{ej} from an atom in thermal equilibrium at temperature T the Doppler effect contributes a width [33]

$$W = \sqrt{11.1\,\gamma_M kTE_{ej}}, \tag{1}$$

where γ_M is the ratio of the electron to the atomic mass and k is Boltzmann's constant. The autoionizing region of He is particularly affected because of the small atomic mass and the large ejected electron energies of ~ 35 eV. For helium at 300 K and an ejected electron energy of 35 eV we find $W=37$ meV. If this is added (in quadrature) to our nominal resolution of 40 meV we obtain an upper limit for the effective resolution of 54 meV.

In Sec. III we present the results of fitting generalized line profiles to the spectra. It has been shown that, in the absence of PCI effects and provided none of the resonances overlap, an ejected electron spectrum, observed at angles θ and ϕ, due to charged particle impact will take the form [34]

$$I(E,\theta,\phi) = \sum_{\mu} \frac{\alpha_\mu \eta_\mu + \beta_\mu}{1+\eta_\mu^2} + \gamma, \tag{2}$$

where the sum is over the autoionizing levels labeled by μ, and the ejected electron energy E enters via the definition $\eta_\mu = 2(E-E_\mu)/\Gamma_\mu$, which is the energy, in half-widths $(\Gamma_\mu/2)$, away from the μ^{th} resonance position E_μ [35]. The parameters $\alpha_\mu(\theta,\phi)$ and $\beta_\mu(\theta,\phi)$ depend on the collision dynamics and describe a resonance line profile. The parameter $\gamma(E,\theta,\phi)$ describes the direct ionization background and is a slowly varying function of E. We found that the empirical function

$$\gamma = \gamma' + \frac{\gamma''}{E}, \tag{3}$$

where γ', γ'' are constants for a given spectrum, gave an excellent fit to all the data. When fitting Eq. (2) to our spectra it is necessary to fold in the instrument function. We found that it was not possible to fit both the $n=2$ and $n=3$ regions of a spectrum with a Gaussian-type instrument function: the required width for $n=2$ was too large for the $n=3$ region. In fact we found that a fixed Voigt profile of 48.5 meV full width at half maximum (FWHM), formed by folding a Gaussian of FWHM 46.5 meV with a Lorentzian of FWHM 6.5 meV, gave a good fit to all regions of all the spectra presented in this paper. (It is possible that the Doppler broadening is in some way responsible for this instrument function; in previous experiments on Xe [32] a pure Gaussian was adequate to explain the experimental results.)

III. RESULTS AND DISCUSSION

In principle it is not usually possible to unambiguously assign a feature in an ejected electron spectrum to a particular final ion state; however, He is a special case because the maximum possible ejected electron energy, for a transition leaving the ion in a state $N>1$, is 1 Ry (≈ 13.6 eV), which is the difference between the double-ionization potential (79.0 eV) and the $N=2$ threshold (65.4 eV). Thus for the ejected electron spectra below, which begin at 32 eV, the

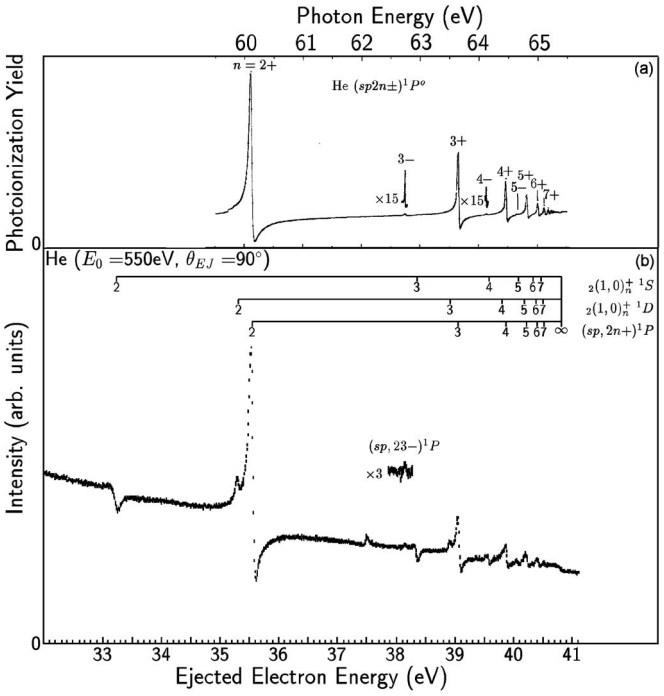

FIG. 2. (a) He photoabsorption spectrum from Ref. [9]. (b) Ejected electron spectrum taken at 90° with respect to a 550 eV incident electron beam.

final ion state is $N=1$. To convert ejected electron energies to level positions we have used a first ionization potential of 24.587 eV.

Below we discuss spectra taken at the three incident electron beam energies 550, 150, and 75 eV, for three ejected electron directions 60°, 90°, and 120° at each energy. There are some general rules that apply to the spectra. (1) 120° seems to be the best angle for seeing nondipole levels at all incident energies. Presumably this is because interference effects between these levels and opposite-parity continua enhance the line shapes relative to those in the 90° spectra. (In contrast, the same effects, with opposite sign, suppress these levels in 60° spectra.) (2) 550 eV spectra show singlets (not triplets that require exchange excitation) of both dipole and nondipole levels. The 150 eV spectra show singlet levels for all n, and show the $n=2$ triplet as a weak feature. In the 150 eV spectra, nondipole singlet levels are enhanced (relative to dipole) when compared with the 550 eV spectra. Therefore the 150 eV spectra are useful for observing and assigning nondipole singlet levels. (3) The 75 eV spectra show both singlet and triplet nondipole levels; comparison with the 150 eV spectra enables the triplet levels to be assigned.

Figure 2(a) shows the He photoabsorption spectrum below the $N=2$ threshold, taken from Ref. [9], in which the optically allowed $(sp,2n\pm)\ ^1P$ levels are labeled. Figure 2(b) shows our survey spectrum for 550 eV incident energy and an ejected 90° with respect to the incident beam direction. Three prominent Rydberg series are present whose lowest members are the well-known $2s^2\ ^1S_0$, $2p^2\ ^1D_2$, and $2s2p\ ^1P_1$

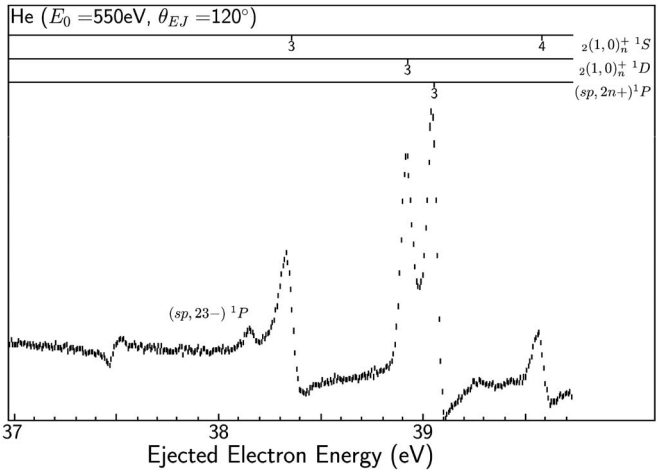

FIG. 3. The $n=3$ region (background subtracted) of an ejected electron spectrum taken at 120° with respect to a 550 eV incident electron beam. The weak $(sp,23-)\ ^1P_1$ level is indicated.

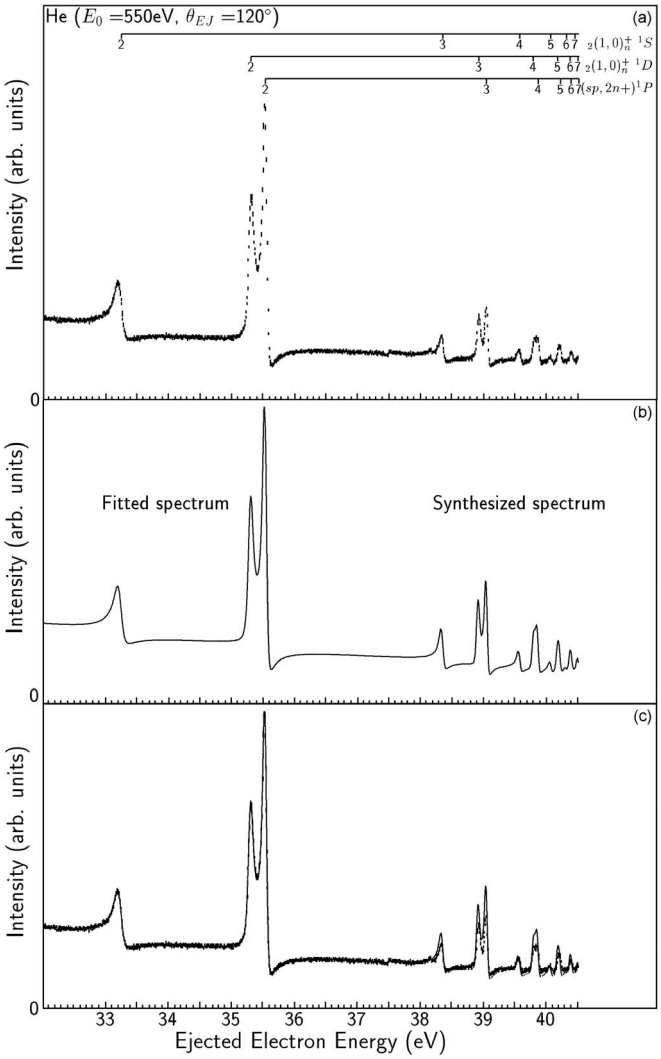

FIG. 4. (a) Ejected electron spectrum taken at 120° with respect to a 550 eV incident electron beam. (b) Left half: $n=2$ spectrum reconstructed from fitting Eq. (2) to the three $n=2$ levels. Right half: $n\geqslant 3$ spectrum synthesized from $n=2$ parameters (see text). (c) shows (b) superimposed on (a).

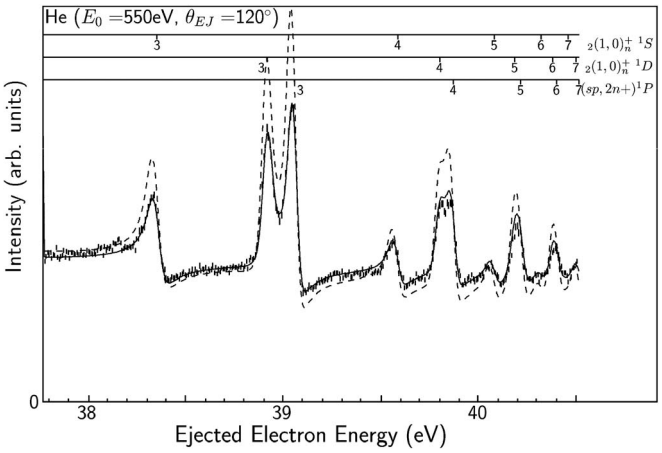

FIG. 5. Closeup of right half of Fig. 4. Dashed line: same as solid line in Fig. 4(b). Solid line: fitted $n=3$ region and synthesized $n \geqslant 4$ region using $n=3$ parameters (see text).

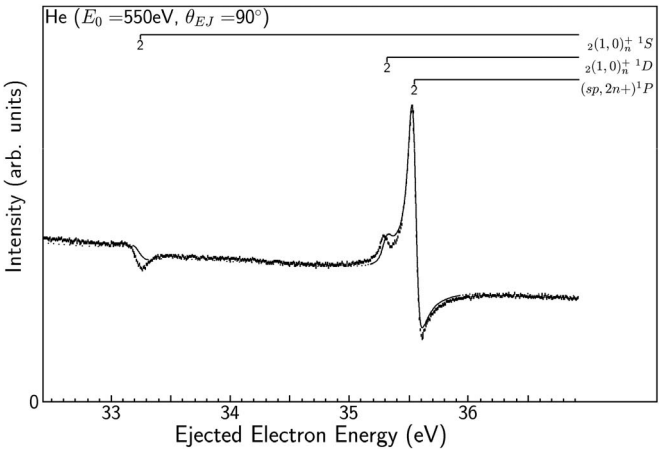

FIG. 7. $n=2$ region of an ejected electron spectrum taken at 90° with respect to a 550 eV incident electron beam. Solid line: Sum of equivalent spectra for 60° and 120° (see text).

autoionizing levels. For the higher members of each series the $(sp,2n\pm)$ scheme is used for the optically allowed series while the ${}_N(K,T)_n^A$ classification scheme is used for most of the optically forbidden series. With our resolution the unresolved Rydberg series appear up to $n=7$; the $^1S_0$ levels may be resolved from the other two up to $n=5$. The level positions indicated for the three series are from Brink *et al.* [7] for $n=2$ and are the theoretical values of Chen [2] for $n>2$. As can be seen, at high incident electron energy and for this ejected electron direction the optically allowed ^1P levels closely mimic the asymmetric profiles of their photoionization counterparts in Fig. 2(a); the reason for this is discussed below. Also present in Fig. 2(b) are two other features: the $2p^2\ ^1S_0$ level at about 37.5 eV, and the very weak $(sp,23-)\ ^1P_1$ level; this is the first time to our knowledge that the latter has been seen in an electron impact experiment.

The $(sp,23-)\ ^1P_1$ level may be seen more clearly in Fig. 3 which shows a high-quality, background-subtracted spectrum of the $n=3$ region for an incident energy of 550 eV and an ejected electron direction of 120°. In the electron impact spectrum the $(sp,23-)\ ^1P_1$ level is about 22 times weaker than the $(sp,23+)\ ^1P_1$ level, in qualitative agreement with the photoabsorption ratio of about 1/30.

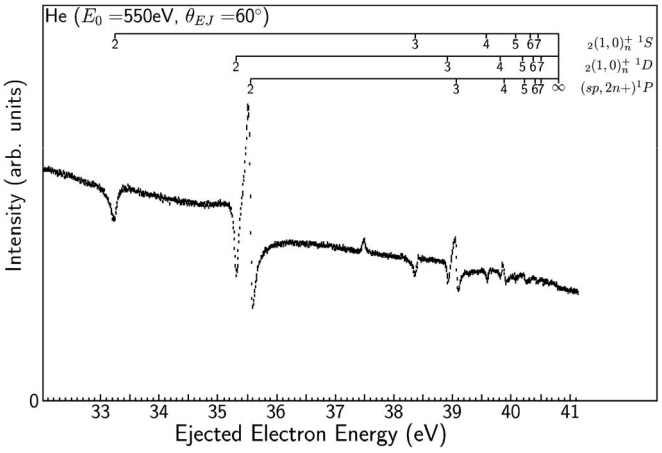

FIG. 6. Ejected electron spectrum taken at 60° with respect to a 550 eV incident electron beam. The feature at 37.5 eV is $2p^2\ ^1S_0$.

Figure 4(a) shows a survey ejected electron spectrum for 550 eV incident energy and an ejected electron direction of 120°. The line profiles for the $^1S_0$ and $^1D_2$ levels are dramatically different from those for 90°. As in Fig. 2 the line profiles of the lowest members of each series are repeated for the higher members of the series. This is to be expected for a well-behaved Rydberg series of autoionizing levels, where both the widths and the excitation probabilities scale in the same way with principal quantum number. The left half of Fig. 4(b) shows the results of a least-squares fit of Eq. (2) to the three $n=2$ levels. The resulting three sets of line profile parameters α_μ,β_μ, and the common parameter $\gamma(E)$, together with Chen's calculated values [2] of the positions and widths of all levels, were then used to synthesize the spectrum in the right half of the figure. Figure 4(c) shows (b) superimposed on (a). The shape of the $n \geqslant 3$ series is correctly given by the synthesized spectrum but the magnitude is too large. Note that the apparent change in the ratio of the ^1D to the ^1P intensity with increasing n is in fact due to the finite experimental resolution—the n^1P levels are narrower than the n^1D levels and hence their height appears to decrease more rapidly with increasing n; with perfect resolution a well-behaved Rydberg series has an n-independent peak intensity. This region is shown in more detail in Fig. 5 with the synthesized spectrum of Fig. 4(b) given by the broken curve. The solid curve is given by the same procedure as in Fig. 4, but using a fit to the $n=3$ levels. The agreement of the synthesized $n \geqslant 4$ spectrum with the experimental spectrum is very good, from which it may be deduced that the electron impact excitation matrix elements for $n \geqslant 3$ scale approximately as expected for well behaved Rydberg series.

Figure 6 shows a survey ejected electron spectrum for 550 eV incident energy and an ejected electron direction of 60°. The line profiles are very different from both the 90° and 120° spectra in Figs. 2 and 4, respectively. Almost all nondipole levels for 60° have a mainly "window" resonance character—a notable exception is $2p^2\ ^1S_0$ at 37.5 eV [the lowest member of the ${}_2(-1,0)_n^+\ ^1S$ series] which is enhanced

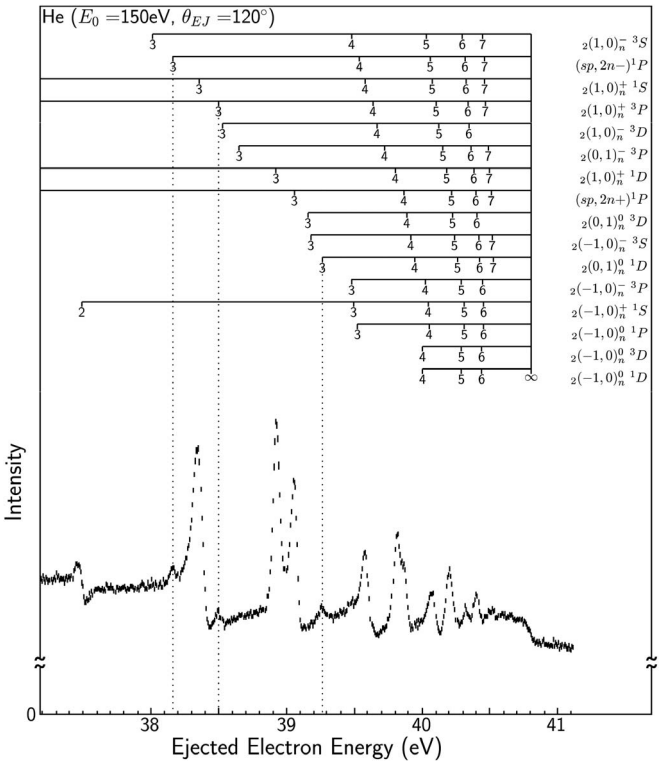

FIG. 8. $n \geqslant 3$ region of an ejected electron spectrum taken at 120° with respect to a 150 eV incident electron beam.

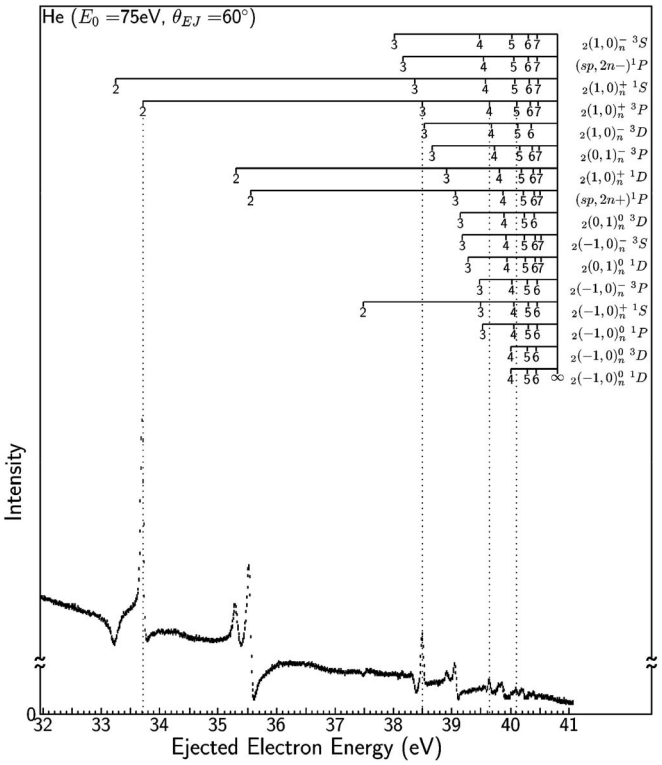

FIG. 9. Ejected electron spectrum taken at 60° with respect to a 75 eV incident electron beam. Note the prominent triplet levels indicated by the vertical dotted lines.

relative to its appearance in the other two spectra.

As stated above, we ascribe the differences between the line shapes in the three spectra to interference effects between autoionizing levels and opposite-parity continua which change sign for ejected electrons 180° apart. A detailed discussion of such interference effects is given in Ref. [36] in the context of Xe ejected electron spectra, and in Ref. [23] for He $(e,2e)$ spectra. For the Xe spectra we found that the summation of spectra for ejected electron directions 50° and 130° removed the interference terms and resulted in a spectrum almost identical to the 90° spectrum; clearly it is of interest to see if the same is true of He. In order to do this, the $n=2$ portions of the 120° and 60° data in Figs. 4 and 6 were fitted to Eq. (2) and the summed spectrum created by adding the two sets of α, β, γ. This procedure was necessary in order to align the energy scales of the spectra as accurately as possible; it was found that even a small misalignment profoundly affected the summed spectrum. The summed spectrum is shown in Fig. 7. As can be seen it is very similar to the 90° data; in particular the asymmetry of the ^1P level is almost identical in the summed and 90° spectra. Note that for the line profiles to be n independent requires that the interference effects which lead to the highly angular-dependent spectral shapes must scale the same way with energy (i.e., n) which in turn implies that the electron impact direct ionization matrix elements for all multipoles scale the same way with energy.

Figure 8 shows the mainly $n \geqslant 3$ portion of a spectrum for 150 eV incident energy and 120° ejected electron direction. Three weak features are indicated by vertical dotted lines. The first of these is the $(sp, 23-)\ ^1P_1$ level with an intensity

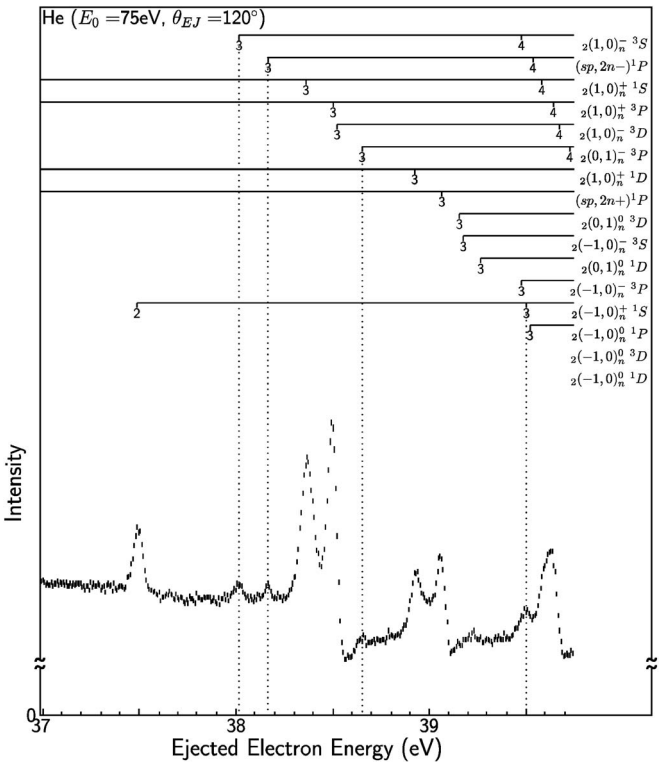

FIG. 10. $n=3$ region of an ejected electron spectrum taken at 120° with respect to a 75 eV incident electron beam.

TABLE I. He autoionizing levels below the $N=2$ threshold seen in the present work. Theoretical values are a compilation from Refs. [2,37–47] (see text). The remaining columns in the table are other workers' experimental values [5,12,18,30,31]. The numbers in parentheses are the uncertainties in the last digits: 0.138(15) means 0.138±0.015. Level energies used for calibration are in parentheses.

			Config-	This work		Theory		[a] Ref.[18], [b] Ref.[31]		[c] Ref.[12], [d] Ref.[5]		Ref.[30]
μ	State	Term	uration	E (eV)	Γ (eV)	E (eV)	Γ (eV)	E (eV)	Γ (eV)	E (eV)	Γ (eV)	E (eV)
	$n=2$											
1	$_2(1,0)_2^+$	$^1S^e$	$2s^2$	57.839(12)	0.120(14)	57.833(8)	0.1076(170)	57.82(4)[a]	0.138(15)			57.84(15)
2	$_2(1,0)_2^+$	$^3P^o$	$2s2p$	58.302(8)	0.005(11)	58.312(1)	0.0082(0)	58.30(3)[a]	<0.015			58.31(3)
3	$_2(1,0)_2^+$	$^1D^e$	$2p^2$	59.903(8)	0.052(21)	59.950(45)	0.0676(34)	59.89(3)[a]	0.072(18)	59.905(5)[c]	0.057(3)	59.85(9)
4	$_2(1,0)_2^+$	$^1P^o$	$2s2p$	60.144(8)	0.037(7)	60.149(5)	0.0368(6)	(60.130)[a]	0.042(18)	60.147(4)[d]	0.037(1)	60.09(6)
	$n=3$											
5	$_2(1,0)_3^+$	$^1S^e$	$2s3s$	62.956(8)	0.033(10)	62.953(1)	0.0314(62)	62.94(3)[a]	0.041(10)			62.97(6)
6	$_2(1,0)_3^+$	$^3P^o$	$sp,23+$	63.095(12)	0.003(2)	63.096(0)	0.0022(1)	63.07(3)[a]				63.11(2)
7	$_2(1,0)_3^+$	$^1D^e$	$2p3p$	63.515(9)	0.012(8)	63.529(13)	0.0161(10)	63.50(3)[a]				63.51(4)
8	$_2(1,0)_3^+$	$^1P^o$	$sp,23+$	(63.658)	0.007(5)	63.657(1)	0.0083(1)	63.65(3)[a]		63.658(4)[d]	0.010(1)	
	$n=4$											
9	$_2(1,0)_4^+$	$^1S^e$	$2s4s$	64.184(8)	0.013(8)	64.178(0)	0.0123(13)	64.18(3)[a]				
10	$_2(1,0)_4^+$	$^3P^o$	$sp,24+$	64.229(8)		64.234(0)	0.0008(0)	64.23(3)[a]				
11	$_2(1,0)_4^+$	$^1D^e$	$2p4p$	64.400(8)		64.408(8)	0.0068(5)	64.39(3)[a]				64.44(2)
12	$_2(1,0)_4^+$	$^1P^o$	$sp,24+$	64.469(8)		64.465(1)	0.0034(1)	64.45(3)[a]		64.467(4)[d]	0.0040(5)	
	$n=5$											
13	$_2(1,0)_5^+$	$^1S^e$	$2s5s$	64.682(8)		64.673(2)	0.0058(5)	64.67(4)[a]				} 64.85(2)
14	$_2(1,0)_5^+$	$^3P^o$	$sp,25+$	64.696(8)		64.700(0)	0.0004(0)	64.69(4)[a]				
15	$_2(1,0)_5^+$	$^1D^e$	$2p5p$	64.804(23)		64.789(9)	0.0034(2)					
16	$_2(1,0)_5^+$	$^1P^o$	$sp,25+$	64.822(8)		64.814(0)	0.0018(0)			64.816(4)[d]	0.0020(3)	
	$n=6$											
17	$_2(1,0)_6^+$	$^1S^e$	$2s6s$	} 64.924(12)		64.924(5)	0.0021(15)					} 65.04(2)
18	$_2(1,0)_6^+$	$^3P^o$	$sp,26+$			64.934(0)	0.0002(0)					
19	$_2(1,0)_6^+$	$^1D^e$	$2p6p$	} 64.992(9)		64.988(9)	0.0021(3)					
20	$_2(1,0)_6^+$	$^1P^o$	$sp,26+$			64.999(0)	0.0010(0)					
	$n=7$											
21	$_2(1,0)_7^+$	$^1S^e$	$2s7s$	} 65.096(15)		65.059(1)	0.0019(0)					
22	$_2(1,0)_7^+$	$^3P^o$	$sp,27+$			65.067(0)	<0.0001					
23	$_2(1,0)_7^+$	$^1D^e$	$2p7p$			65.096(1)	0.0012(0)					
24	$_2(1,0)_7^+$	$^1P^o$	$sp,27+$			65.108(1)	0.0006(0)					
25	$_2(-1,0)_2^+$	$^1S^e$	$2p^2$	62.093(12)	0.007(7)	62.097(24)	0.0117(59)	62.06(3)[a]				62.08(2)
26	$_2(-1,0)_3^+$	$^1S^e$	$2p3p$	64.088(16)		64.094(3)	0.0045(24)					
27	$_2(1,0)_3^-$	$^3S^e$	$2p3p$	62.603(13)		62.608(0)	0.0002(0)					
28	$_2(1,0)_3^-$	$^1P^o$	$sp,23-$	62.748(10)		62.758(0)	0.0001(0)	62.759(2)[b]		62.758(4)[d]	0.0005(3)	62.79(2)
29	$_2(0,1)_3^-$	$^3P^o$	$sp,23-$	63.241(29)		63.249(0)	<0.0001	63.247(2)[b]				
30	$_2(0,1)_3^0$	$^1D^e$	$2s3d$	63.855(8)	0.008(8)	63.876(12)	0.0004(1)					

[a] Reference [18]
[b] Reference [31]
[c] Reference [12]
[d] Reference [5]

relative to $(sp,23+)\ ^1P_1$ similar to that seen at 550 eV incident energy. The second is the $_2(1,0)_3^{+\ 3}P$ level; this lies close to the $_2(1,0)_3^{-\ 3}D$ level, but the latter is expected to be absent at this incident energy. The third is a previously unseen quadrupole level, the first $(n=3)$ member of the $_2(0,1)_n^{0\ 1}D$ series.

Figure 9 is a survey spectrum for 75 eV incident energy and ejected electron direction of 60°. As stated in the introduction of this section, for this direction destructive interference suppresses many series; an exception is the $_2(1,0)_n^{+\ 3}P$ series which stands out from the adjacent $_2(1,0)_n^{+\ 1}S$ series, and hence may be resolved up to $n=5$, as indicated in the figure. At this incident energy the main $L=1$ triplet and singlet series, $_2(1,0)_n^{+\ 3}P$ and $(sp,2n+)\ ^1P_1$, are of comparable intensity; i.e., exchange processes are of equal importance to direct processes. Figure 10 shows the (mainly) $n=3$ region for 120° where four weak features of similar intensity are identified. The first and third are the lowest members $(n=3)$ of the previously unobserved $_2(1,0)_n^{-\ 3}S$ and $_2(0,1)_n^{-\ 3}P$ series. The second is the $(sp,23-)\ ^1P_1$ level seen in the spectra for all incident energies. The fourth feature peaks at an energy that corresponds almost exactly with the calculated $_2(-1,0)_3^{+\ 1}S$ (i.e., $2p3p\ ^1S$) level. This feature appears in a number of other spectra and in all cases its line shape closely mimics that of the well-resolved $2p^2\ ^1S$ level whose asymmetry is a strong function of incident electron energy and ejected electron emission angle. We therefore deduce that the levels that are calculated to lie on either side of the $2p3p\ ^1S$ level (see Fig. 10) do not contribute significantly to this feature.

A series of least-squares fits to the generalized line profile Eq. (2) were carried out to obtain the positions and (where possible) the widths of the levels in the spectra. Table I lists all the levels that have been observed in this work; for easy reference the first column assigns them a label $\mu=1\rightarrow30$. Our energy scale was aligned using level $\mu=8$, $(sp,23+)\ ^1P$, which was fixed at the photoionization value [5]. (This level was chosen, rather than the more intense level $\mu=4$, $2s2p\ ^1P$, in order to obviate the possibility of inaccuracies due to PCI effects; these are proportional to the natural width of a level [26] and for $n=2$ the ^1P width is 37 meV whereas for $n=3$ the width is only 8 meV.) Relative energies were then determined from the increase of energy of 7.5 meV between points set by an in-house computer-controlled digital-to-analog converter.

The energies and widths given in Table I are the average values from fits to all of the nine spectra (the combinations of $E_0=550$, 150, and 75 eV and $\theta_{EJ}=60°$, 90°, and 120°) in which a level could be seen. Since the positions given are those found from fits to the generalized line profile, they are resonance positions rather than peak positions; exceptions are listed below. The uncertainties given are the standard deviations among the fits except that there is a minimum uncertainty of 8 meV in our absolute energy scale. Widths not given in the table were too narrow to fit and were fixed at theoretical values [2] in the fits.

The upper part of the table consists of the four Rydberg series whose lowest members $(\mu=1\rightarrow4)$ are the four lowest-energy $2\ell2\ell'$ levels. It was found that if all α_μ,β_μ in Eq. (2)

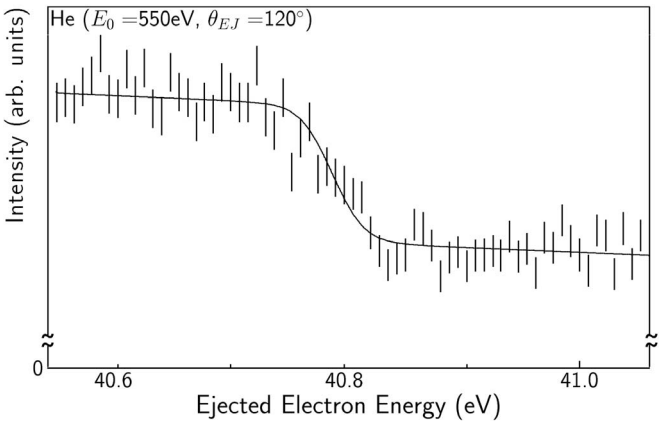

FIG. 11. Intensity step near the $N=2$ threshold in an ejected electron spectrum taken at 120° with respect to a 550 eV incident electron beam. The solid line is a fit that includes a step function folded with the experimental energy resolution.

were independently fitted parameters, the fits were rather ambiguous because very small changes in χ^2 were accompanied by large changes in all fitted parameters for $n=4,5$. We attribute this to the fact that these levels are not well resolved. The discussion above relating to Fig. 4 suggested a way around this problem and satisfactory fits with reduced $\chi^2<2$ were obtained by fixing α_μ,β_μ values for $n=4,5$ $(\mu=9\rightarrow16)$ at the values fitted for the corresponding well resolved $n=3$ levels $(\mu=5\rightarrow8)$. For $n=6$ there were two groups of two unresolved levels $(\mu=17,18$ and $\mu=19,20)$; the peak positions of these features are given in the table. For $n=7$ the four levels $(\mu=21\rightarrow24)$ appeared as a single unresolved feature whose peak position is given in the table.

The lower part of the table consists of other levels seen in this work which have been discussed in Figs. 8 and 10. The widths of very narrow levels were fitted with large uncertainties. Thus, for example, level $\mu=25$ yields a width 0.007(7) eV which essentially provides an upper limit of 0.014 eV.

The theoretical levels and widths in the table are compiled from Refs. [2,37–47]. The values are given as the central value of all the calculations, with an "uncertainty" corresponding to the range of the calculations. Thus, for example, 57.833(8) eV means that the minimum calculated value is 57.825 eV, and the maximum value is 57.841 eV; all other calculations lie between these values. Where necessary, values have been converted using an atomic unit of energy $2\times13.603\ 83$ eV and a double-ionization potential of 79.003 eV [5]. It can be seen that, with the exception of the two lowest $2pnp\ ^1D$ levels, the spread of the theoretical values is less than our experimental uncertainties; overall, there is excellent agreement between theory and experiment.

Also shown in the table are experimental levels taken from other workers. Our values for $(sp,2n+)\ ^1P$ $(n=2,4,5)$ are in excellent agreement with the photoionization values [5] which confirms the linearity and accuracy of our energy scale. Our electron impact results represent an increase in precision over the early electron impact data of Hicks and Comer [18]. The data of Iemura *et al.* [30] include PCI shifts and we have used their estimated shifts as uncer-

tainties in the level positions; there is then good agreement with our values.

Lastly, all the spectra contained a sharp reduction in intensity at, or close to, the $N=2$ threshold. This is due to the end of the quasicontinuum formed by the $n \approx 8 \rightarrow \infty$ unresolved members of the $2\ell n\ell'$ Rydberg series. We fitted this region of the spectrum by modifying Eq. (3) to include a step whose position and magnitude (folded with our energy instrument function) were two extra fitted parameters. Figure 11 (solid line) shows an example of such a fit. Similar fits were carried out for other spectra and gave an average value of 65.377(20) eV for the ionization threshold, just over one standard deviation less than the accepted value of 65.402 eV [5]. It is possible that this disagreement is caused by significant (10%) radiative damping effects that are predicted in the near-threshold ionization yield [6]; i.e., fluorescence of the doubly excited levels becomes about 10% as important as autoionization and causes a corresponding decrease in intensity which, when folded with our instrument function, may lead to a fitted step at an energy slightly below the true threshold.

IV. SUMMARY AND CONCLUSIONS

We have obtained high-quality electron impact ejected electron spectra over a wide range of incident energies and ejected electron directions. The four prominent autoionizing Rydberg series, $^1S, ^3P, ^1D, ^1P$, have been tabulated up to $n=5$ and observed, but not resolved, up to $n=7$. It has been verified that for $n \geqslant 3$ the profile parameters are approximately n independent. The very weak optically allowed $(sp,23-)\ ^1P$ level and the optically forbidden $(sp,23-)\ ^3P$ have been observed. Also, three optically forbidden levels have been seen for the first time. The overall conclusion of this work is that theory does a good job of calculating the positions and widths of all levels we have observed; in all cases there is no discrepancy within our experimental uncertainty.

ACKNOWLEDGMENTS

The authors wish to thank Dr. Peter van der Burgt for sharing his extensive compilation of data on, and references to, He energy levels, and Dr. Thomas Gorczyca for helpful discussions on near-threshold damping effects. This work was supported by the United States National Science Foundation under Grant No. PHY-9987861.

[1] J. W. Cooper, U. Fano, and F. Prats, Phys. Rev. Lett. **10**, 518 (1963).
[2] M.-K. Chen, Phys. Rev. A **56**, 4537 (1997).
[3] D. R. Herrick and O. Sinanoğlu, Phys. Rev. A **11**, 97 (1975).
[4] C. D. Lin, Phys. Rev. A **29**, 1019 (1984); Adv. At. Mol. Phys. **22**, 77 (1986).
[5] M. Domke, K. Schulz, G. Remmers, G. Kaindl, and D. Wintgen, Phys. Rev. A **53**, 1424 (1996).
[6] T. W. Gorczyca, J.-E. Rubensson, C. Såthe, M. Ström, M. Agåker, D. Ding, S. Stranges, R. Richter, and M. Alagia, Phys. Rev. Lett. **85**, 1202 (2000).
[7] J. P. van den Brink, G. Nienhuis, J. van Eck, and H. G. M. Heideman, J. Phys. B **22**, 3501 (1989).
[8] R. P. Madden and K. Codling, Phys. Rev. Lett. **10**, 516 (1963).
[9] M. Domke, C. Xue, A. Puschmann, T. Mandel, E. Hudson, D. A. Shirley, G. Kaindl, C. H. Greene, H. R. Sadeghpour, and H. Petersen, Phys. Rev. Lett. **66**, 1306 (1991).
[10] K. Schulz, G. Kaindl, M. Domke, J. D. Bozek, P. A. Heimann, A. S. Schlachter, and J. M. Rost, Phys. Rev. Lett. **77**, 3086 (1996), and references therein.
[11] A. Menzel, S. P. Frigo, S. B. Whitfield, C. D. Caldwell, and M. O. Krause, Phys. Rev. A **54**, 2080 (1996).
[12] B. Krässig, E. P. Kanter, S. H. Southworth, R. Guillemin, O. Hemmers, D. W. Lindle, R. Wehlitz, and N. L. S. Martin, Phys. Rev. Lett. **88**, 203002 (2002).
[13] J. R. Harries, J. P. Sullivan, J. B. Sternberg, S. Obara, T. Suzuki, P. Hammond, J. Bozek, N. Berrah, M. Halka, and Y. Azuma, Phys. Rev. Lett. **90**, 133002 (2003).
[14] C. Såthe, M. Ström, M. Agåker, J. Söderström, J.-E. Rubensson, R. Richter, M. Alagia, S. Stranges, T. W. Gorczyca, and F. Robicheaux, Phys. Rev. Lett. **96**, 043002 (2006).
[15] K. C. Prince, M. Coreno, R. Richter, M. de Simone, V. Feyer, A. Kivimäki, A. Mihelič, and M. Žitnik, Phys. Rev. Lett. **96**, 093001 (2006).
[16] J. Arol Simpson, G. E. Chamberlain, and S. R. Mielczarek, Phys. Rev. **139**, A1039 (1965).
[17] N. Oda, F. Nishimura, and S. Tahira, Phys. Rev. Lett. **24**, 42 (1970).
[18] P. J. Hicks and J. Comer, J. Phys. B **8**, 1866 (1975).
[19] D. G. McDonald and A. Crowe, J. Phys. B **25**, 2129 (1992).
[20] A. Crowe, D. G. McDonald, S. E. Martin, and V. V. Balashov, Can. J. Phys. **74**, 736 (1996).
[21] M. J. Brunger, O. Samardzic, A. S. Kheifets, and E. Weigold, J. Phys. B **30**, 3267 (1997).
[22] O. Samardzic, L. Campbell, M. J. Brunger, A. S. Kheifets, and E. Weigold, J. Phys. B **30**, 4383 (1997).
[23] B. A. deHarak, J. G. Childers, and N. L. S. Martin, J. Electron Spectrosc. Relat. Phenom. **141**, 75 (2004).
[24] H. B. van Linden van den Heuvell, W. van de Water, H. G. M. Heideman, J. van Eck, and L. Moorman, J. Phys. B **13**, 2475 (1980).
[25] P. J. Hicks, S. Cvejanović, J. Comer, F. H. Read, and J. M. Sharp, Vacuum **24**, 573 (1974).
[26] R. Morgenstern, A. Niehaus, and U. Thielmann, J. Phys. B **10**, 1039 (1977).
[27] P. W. Arcuni, Phys. Rev. A **33**, 105 (1986).
[28] P. W. Arcuni and D. Schneider, Phys. Rev. A **36**, 3059 (1987).
[29] P. Moretto-Capelle, D. Bordenave-Montesquieu, A. Bordenave-Montesquieu, A. L. Godunov, and V. A. Schipakov, Phys. Rev. Lett. **79**, 5230 (1997).
[30] K. Iemura, S. Ohtani, H. Suzuki, J. Takeda, S. Machida, K. Tanabe, T. Takayanagi, K. Wakiya, M. Sekiguchi, Y. Kanai, S.

Kitazawa, X. M. Tong, D. Kato, S. Sakaguchi, T. Watanabe, and F. J. Currell, Phys. Rev. A **64**, 062709 (2001).
[31] P. Baltzer and L. Karlsson, Phys. Rev. A **38**, 2322 (1988).
[32] J. G. Childers, D. B. Thompson, and N. L. S. Martin, Phys. Rev. A **64**, 062703 (2001).
[33] P. J. Chantry, J. Chem. Phys. **55**, 2746 (1971).
[34] B. W. Shore, J. Opt. Soc. Am. **57**, 881 (1967).
[35] U. Fano, Phys. Rev. **124**, 1866 (1961).
[36] J. G. Childers, B. A. deHarak, and N. L. S. Martin, Phys. Rev. A **69**, 042713 (2004).
[37] D. H. Oza, Phys. Rev. A **33**, 824 (1986).
[38] Y. K. Ho, Z. Phys. D: At., Mol. Clusters **21**, 191 (1991).
[39] Y. K. Ho, Phys. Rev. A **48**, 3598 (1993).
[40] Y. K. Ho, Phys. Rev. A **34**, 4402 (1986).
[41] Y. K. Ho and A. K. Bhatia, Phys. Rev. A **44**, 2895 (1991).
[42] D. Wintgen and D. Delande, J. Phys. B **26**, L399 (1993).
[43] E. Lindroth, Phys. Rev. A **49**, 4473 (1994).
[44] L. Wu and J. Xi, J. Phys. B **23**, 727 (1990).
[45] M. Venuti, P. Decleva, and A. Lisini, J. Phys. B **29**, 5315 (1996).
[46] A. Macías and A. Riera, Phys. Lett. A **119**, 28 (1986).
[47] A. Macías, F. Martín, A. Riera, and M. Yáñez, Phys. Rev. A **36**, 4187 (1987).